# *On the min–max estimation of mean daily temperatures*

**Anastasios A. Tsonis, Xinnong Pan, Geli Wang & Catherine Nicolis**

**Climate Dynamics**
Observational, Theoretical and Computational Research on the Climate System

ISSN 0930-7575
Volume 53
Combined 3-4

Clim Dyn (2019) 53:1981-1989
DOI 10.1007/s00382-019-04757-6

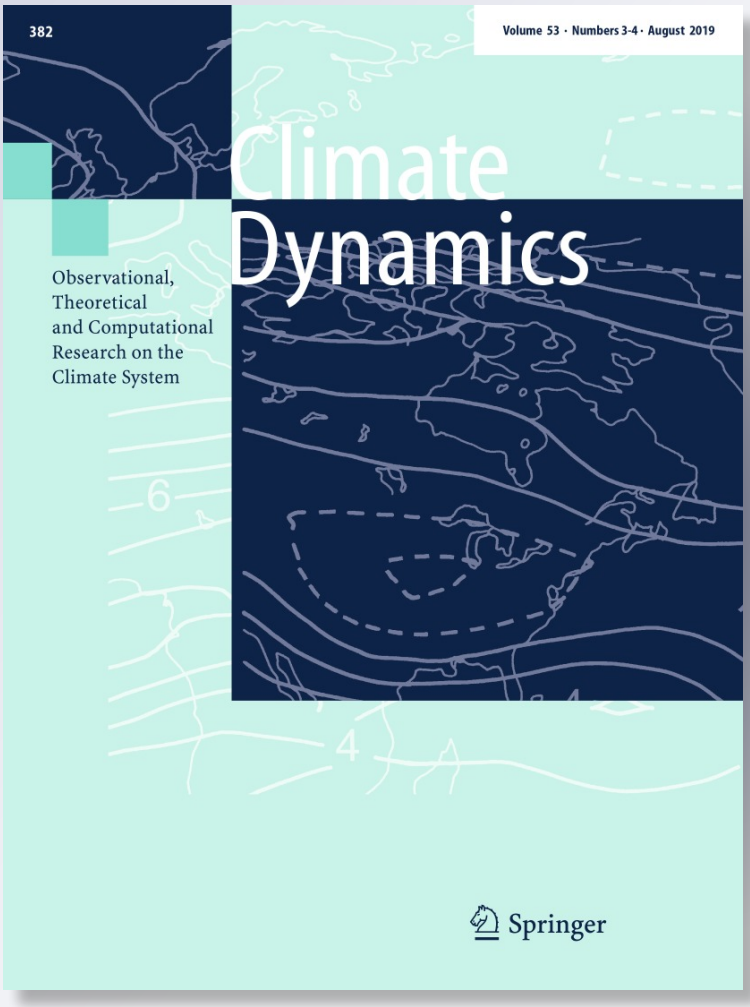


Springer

Climate Dynamics (2019) 53:1981–1989
https://doi.org/10.1007/s00382-019-04757-6

# On the min–max estimation of mean daily temperatures

**Anastasios A. Tsonis[1,2] · Xinnong Pan[3,4] · Geli Wang[3] · Catherine Nicolis[5]**

Received: 8 December 2018 / Accepted: 1 April 2019 / Published online: 11 April 2019


**Abstract**
Modern data analyses of hourly temperature records reveal the existence, in addition to the daily cycle, of multiple forcings of different frequencies. As a result the routine approach of estimating daily local mean temperature directly from the average of the minimum and maximum is heavily compromised. A simple dynamical model subjected to two periodic forcings of different frequencies, amplitudes and phases is solved analytically and shown to induce substantial deviations from the min–max method that depend crucially on the values of the parameters involved.

**Keywords** Mean daily temperature · Slow feature analysis · Driving forces

## 1 Introduction

There is a widely spread conviction that a reliable estimate of the average daily temperature is provided by the sum of the maximum ($T_{max}$) and the minimum ($T_{min}$) values attained over a day, divided by 2. Some doubts on the general validity of this property supported by data have been formulated (see for instance Dall'Amico and Horsteiner 2006; Ma and Guttorp 2013; Bernhardt et al. 2018), but so far there is lack of understanding of the mechanisms behind such deviations.

Obviously, a min–max estimation is rigorously valid if the daily temperature variability happens to be harmonic, i.e., a sinusoidal with a period equal to the daily cycle. Conversely, deviations are to be expected in presence of anharmonicity, i.e., extra forcings of temperature anomaly other than the one of the classic daily cycle. Such forcings may originate from different mechanisms such as the interference of several external independent cycles or nonlinearities, including the fundamentally chaotic nature of atmospheric variability. On the other hand, since we are dealing here with short-scale processes it seems unlikely that nonlinearities will play a role. Everything will therefore happen as if the system is operating around some well-defined reference state.

In Sect. 2 we perform an hourly temperature data analysis which establishes beyond doubt that indeed more than one forcing is present in the temperature records. In Sect. 3 we explore the properties of the simplest deviation from a linear model subjected to just a sinusoidal forcing: that of a linear model subjected to two forcings of different frequencies and amplitudes. This model is quantitatively formulated and solved analytically, providing the instantaneous value of temperature. This value is averaged over the daily cycle and the results are cast as a function of the period of the second cycle and the amplitudes and phases of the two forcings. Some clear-cut deviations from min–max property are detected and their parameter dependencies are analyzed. The main conclusions are summarized in Sect. 4.

## 2 Data analysis and results

In order to delineate possible multiple forcings in the hourly temperature data we employed the method Slow Feature Analysis (SFA). SFA is a procedure for extracting slowly varying driving forces from a given nonstationary time

**Electronic supplementary material** The online version of this article (doi:https://doi.org/10.1007/s00382-019-04757-6) contains supplementary material, which is available to authorized users.

✉ Anastasios A. Tsonis
aatsonis@uwm.edu

[1] Department of Mathematical Sciences, Atmospheric Sciences Group, University of Wisconsin-Milwaukee, Milwaukee, USA

[2] Hydrologic Research Center, San Diego, USA

[3] Key Laboratory of Middle Atmosphere and Global Environment Observation (LAGEO), Institute of Atmospheric Physics, Chinese Academy of Sciences, Beijing, China

[4] University of Chinese Academy of Sciences, Beijing, China

[5] Institut Royal Meteorologique de Belgique, 3 Avenue Circulaire, 1180 Brussels, Belgium

series. Detailed descriptions of this procedure are given in Wiskott and Sejnowski (2002), Wiskott (2003) and Berkes and Wiskott (2005). This approach has successfully been applied in many scientific areas including in climate studies (see for example, Yang et al. 2015).

Slow Feature Analysis is a very involved method which solves the following learning task: Given a multidimensional input signal we wish to find instantaneous scalar input–output functions that generate output signals that vary as slowly as possible but still carry significant information about the input. To ensure the latter we require the output signals to be uncorrelated and have unit variance. In mathematical terms, this can be stated as follows (Wiskott and Sejnowski 2002):

Given an n-dimensional input signal $\mathbf{x}$(t), find a set of real-valued input–output functions $g_j(\mathbf{x})$ such that the output signals

$y_j(t) := g_j(\mathbf{x}(t))$.

Minimize $\Delta(y_i) :=< \dot{y}_j^2 >_t$, under the constraints $<y_j>_t = 0$ (zero mean), $<y_j^2>_t = 1$ (unit variance), $\forall i < j: <y_i y_j>_t = 0$ (decorrelation and order), with $<\bullet>_t$ and $\dot{y}$ indicating temporal averaging and the derivative of $y$, respectively.

The $\Delta$-value is a measure of the temporal slowness of the signal $y(t)$. It is given by the mean square of the signal's temporal derivative. Small $\Delta$-values indicate slowly varying signals. The first two constraints avoid the trivial constant solution and the last guarantees that different output functions $g_j$ code for different information in the input signal. For a tutorial on this method the reader should consult Wiskott and Sejnowski (2002) or a recent presentation in Wiskott et al. (2011). In that tutorial, a simple example of a two-dimensional input signal $x_1(t) = \sin(t) + \cos(11t)^2$ and $x_2(t) = \cos(11t)$ is considered. Both components are quickly varying, but hidden in the signal is the slowly varying 'feature' $y(t) = x_1(t) - x_2(t)^2 = \sin(t)$ which can be extracted with a polynomial of degree two, namely $h(\boldsymbol{x}) = x_1 - x_2^2$

In the case of one observable from an unknown system (like in our case) where the actual state space is not known, embedding in some dimension is necessary to delineate the underlying dynamics much like in attractor reconstructions. The formal steps in the procedure are as follows:

Consider a time series $\{x(t)\}$, $t = t_1, \ldots t_n$, where $t$ stands for time and $n$ indicates the length of the time series. First, we embed $\{x(t)\}$ into an $m$-dimensional state space:

$$X(t) = \{x_1(t), x_2(t), \ldots, x_m(t)\} \qquad t = t_1, \ldots t_N,$$

where $N = n - m + 1$. Then nonlinear expansions (usually second-order polynomials) are used to generate a $k$-dimensional function state space:

$$H(t) = \{x_1(t), \ldots x_m(t); x_1^2(t), \ldots, x_1(t)x_m(t); \ldots; x_{m-1}^2(t), x_{m-1}(t)x_m(t); x_m^2(t)\},$$

$t = t_1, \ldots t_N$,

which can also be written as

$$H(t) = \{h_1(t), h_2(t), \ldots, h_k(t)\} \quad t = t_1, \ldots t_N,$$

where $k = m + m(m+1)/2$.

In the third step, the expanded signal $H(t)$ is normalized so that it satisfies the constraints of zero mean and unit variance. This is referred to as whitening or sphering. Thus, we have

$$H'(t) = \{h_1(t), h_2(t), \ldots, h_k(t)\} \quad t = t_1, \ldots t_N,$$

where $h_j' = 0$ (zero mean), $h_j' h_j'^T = 1$ (unit variance), $h_j'(t) = \left(h_j(t) - \overline{h_j}\right)/\mathrm{S}$ and $S = \frac{1}{K}\sqrt{\sum_{j=1}^{k}\left(h_j(t) - \overline{h}\right)^2}$

Then, by using Schmidz algorithm, $H'(t)$ is orthogonalized into:

$$Z(t) = \{z_1(t), z_2(t), \ldots, z_k(t)\} t = t_1, \ldots t_N.$$

Thus, each output signal can be expressed as the following linear combination:

$$y(t) = a_1 z_1(t) + a_2 z_2(t) + \ldots + a_k z_k(t),$$

where $(a_1, a_2, \ldots, a_k)$ is a set of weighting coefficients.

Note that the output signals are orthogonal and nontrivial, i.e.:

$$z_i(t) z_j(t) = 0, \quad \overline{z}_i(t) = \overline{z}_j(t) = 0, \quad z_j(t) z_j^T(t) = 1.$$

Subsequently, we perform the 1st order differencing on $Z(t)$ to obtain the derivative function space:

$$\dot{z}_j(t_i) = z_j(t_{i+1}) - z_j(t_i),$$

$$\dot{Z}(t) = \left\{\dot{z}_1(t), \dot{z}_2(t), \ldots, \dot{z}_k(t)\right\} \quad t = t_1, \ldots t_N.$$

Then we establish the time-derivative covariance matrix $B = \left(\dot{Z}\dot{Z}^T\right)_{K\times K}$ and calculate its eigenvalues $\lambda_1 \le \lambda_2 \le \ldots \le \lambda_k$ and the corresponding eigenvectors are $W_1, W_2, \ldots, W_k$. Finally, using $W_1$, the slowest driving force can be written as:

$$y_1(t) = rW_1 \times Z_t + c,$$

where $r$ and $c$ are two arbitrary constants resulting from quadrature of $y(t)$ and solution of $W_1$, respectively. Note that the driving force may not necessarily consist of just one component but several components, which, as we will see below, correspond to forcings at certain time scales.

Figure 1 illustrates the method we followed here in order to delineate the driving force and its components. The top panel is the hourly temperature for the month of September 2012 at the Beijing Botanical Garden station. The second panel is the driving force after we applied the

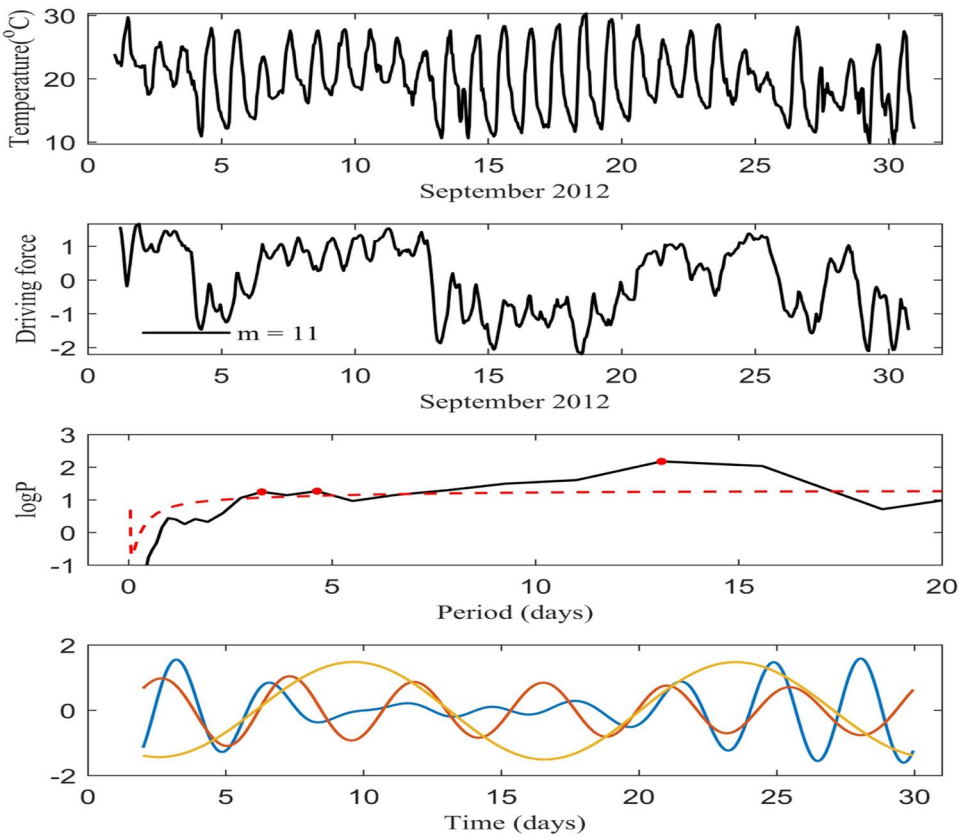


**Fig. 1** From top to bottom: **a** the hourly temperature data for the month of September 2012 at the Beijing Botanical Garden station, **b** the SFA extracted driving force signal, **c** the average the time-averaged power spectrum of the wavelet transform of the SFA extracted driving signal (black solid curve) and the 95% confidence level (red dashed line). The red dots show the periods of the oscillatory components of the driving force that are significant above the 95% level, **d** the oscillatory components of the driving force signal

above algorithm for an embedding dimension $m = 11$ (as explained above this signal is normalized to zero mean and unit variance). The driving force signal may be composed of more than one component. In order to extract the components of the driving force signal we perform a wavelet transform of the driving signal and then we compute the time-averaged power spectrum of the wavelet transform. Here we use the Morlet wavelet (for details see Torrence and Combo 1998). In the third panel the black solid curve is the time-averaged power spectrum of the wavelet transform of the driving force, and the red dashed line is the 95% confidence level. The red dots show the periods of the oscillatory components of the driving force that are significant above the 95% level. Finally, the bottom panel shows the filtered signals corresponding to those oscillatory components (3.3, 4.6, and 13.1 days, respectively). This example demonstrates that there is much more dynamics involved in the temperature record than a simple sinusoidal wave. Furthermore, as Figs. 2, 3, 4 and 5 demonstrate (as in Fig. 1 but for all months in 2012), the significant oscillatory components of the driving force are not the same for all months. We have repeated our analysis for several other stations. For example, see Supplementary Figures S1–S8. Here we need to stress that sampling variability may cause some peaks in Fig. 4 to be significant and others not. Thus, variations in the extracted oscillatory components even between months of the same season (for example, January–February or July–August, Figs. 4 and 5) may not necessarily imply that the dynamics of the driving force are different. A lower confidence interval would probably make the one-day oscillation significant in January and in July. That will also result in more complicated structures in Fig. 5. Be this as it may, the robust and unequivocal conclusion of this analysis is that the forcing structure in each case *is more complex than a simple sinusoid*. Also note that the semi-diurnal (subharmonic) frequency does not appear in the results. This is probably because the approach is geared toward lower than higher frequencies. A final note on the results: if a driving force consists of several components, the predictability of the system itself and different selection of the embedding dimension $m$ might affect the extraction results. We have performed a sensitivity analysis by considering other embedding dimensions. For example, Supplementary Fig. S9 is the same as the second panel in Fig. 1 but it shows the results for both $m = 11$ and $m = 23$. In general, we find that the higher the embedding the smother the driving signals tend to be. However, the complex character of the driving signal remains unaffected. Next, we explore the properties of the simplest deviation from a linear model subjected to just a sinusoidal forcing: that of a linear model subjected to two forcings of different frequencies and amplitudes.

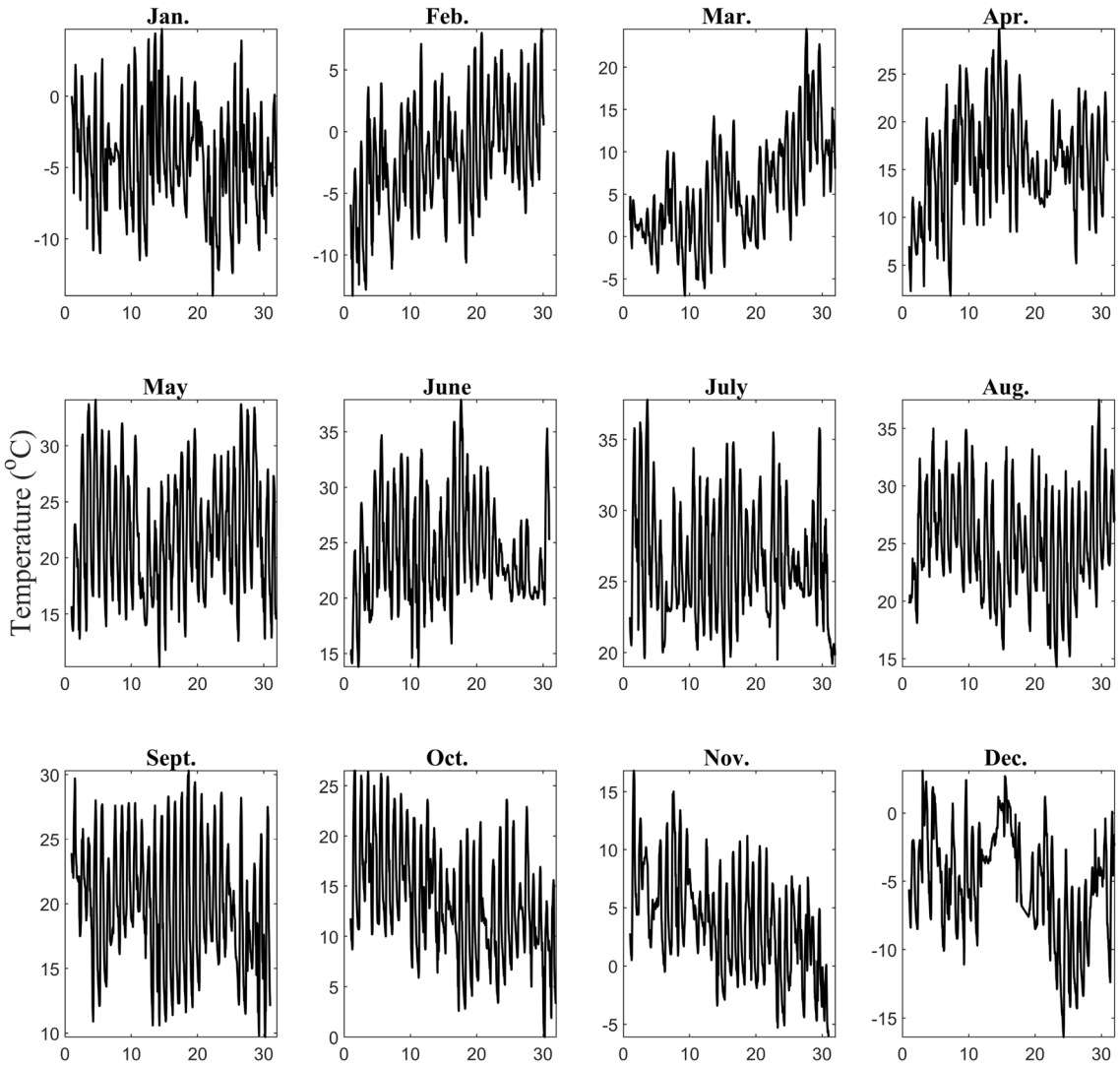


**Fig. 2** Same as Fig. 1 (top panel) but for all months in 2012

## 3 A linear model

Let $x$ be the temperature anomaly around some reference value and $\lambda^{-1}$ the characteristic relaxation time in absence of external forcings. We are interested in the time evolution of $x$ in the presence of two sinusoidal forcings of amplitudes $\varepsilon_1$ $\varepsilon_2$, frequencies $\omega_1$ $\omega_2$ and phases $\varphi_1$ $\varphi_2$, stipulating that the first forcing represents the daily cycle. The equation of the time dependence of $x$ takes thus the form

$$dx/dt = -\lambda x + \varepsilon_1 \cos(\omega_1 t - \phi_1) + \varepsilon_2 \cos(\omega_2 t - \phi_2). \quad (1)$$

It admits in the long time limit the analytic solution

$$x(t) = \frac{\varepsilon_1\left[\lambda\cos\left(\omega_1 t - \phi_1\right) + \omega_1 \sin\left(\omega_1 t - \phi_1\right)\right]}{\lambda^2 + \omega_1^2} + \frac{\varepsilon_2\left[\lambda\cos\left(\omega_2 t - \phi_2\right) + \omega_2 \sin\left(\omega_2 t - \phi_2\right)\right]}{\lambda^2 + \omega_2^2}, \quad (2)$$

or

$$x(t) = \frac{\varepsilon_1 \sin(\omega_1 - \phi_1 + \psi_1)}{\sqrt{\lambda^2 + \omega_1^2}} + \frac{\varepsilon_2 \sin(\omega_2 - \phi_2 + \psi_2)}{\sqrt{\lambda^2 + \omega_2^2}}, \quad (3)$$

with

$$\psi_1 = \arctan(\lambda/\omega_1)$$
$$\psi_2 = \arctan(\lambda/\omega_2). \quad (4)$$

Figure 6 depicts the time evolution of $x(t)$ for $\lambda = 1$, $\varepsilon_1 = \varepsilon_2 = 1$, $\omega_1 = 1/3\pi$, $\omega_2 = \omega_1/10$ and $\varphi_1 = \varphi_2 = 0$. We recognize the rapid oscillation of period $T_1 = 2\pi/\omega_1 = 6$ time units embedded into the slow one of period $T_2 = 60$ time units. The choice of these particular values for the ωs defines a time scale such that $T_1$ is equal to 24 h. From Eq. (3) one notices that for $\omega_2$ close to $\omega_1$ the time dependence of $x$ takes the form of beatings, where a

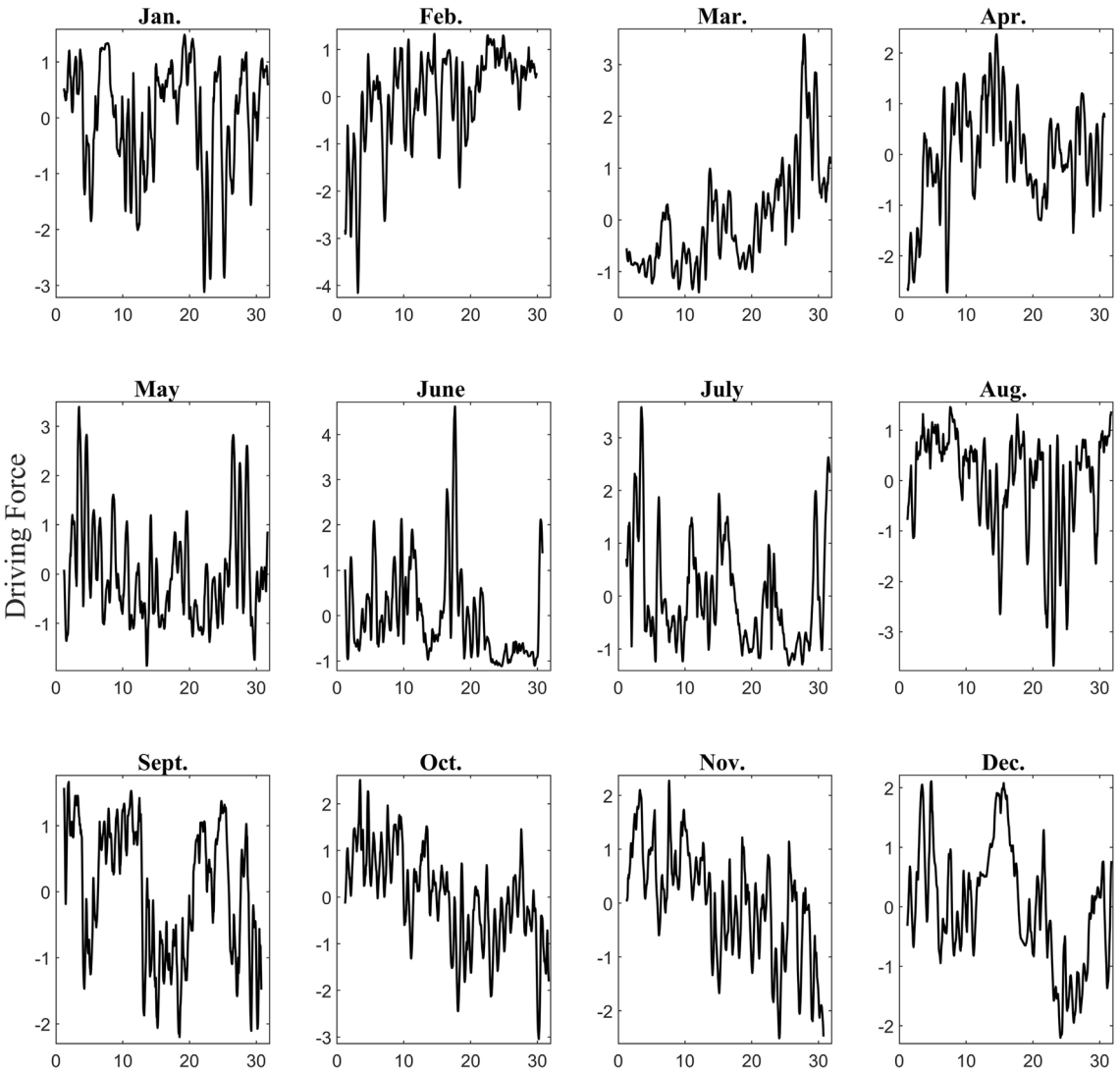


**Fig. 3** Same as Fig. 1 (second panel) but for all months in 2012

rapid oscillation of frequency $(\omega_1+\omega_2)/2$ is modulated by a slowly varying amplitude of frequency $(\omega_1-\omega_2)/2$ (not shown).

Our next step is to compute from the data of Fig. 6 the average value $x$ of the full $x(t)$ over the successive short cycles and, in parallel, to evaluate for each of these cycles $(x_{max}+x_{min})/2$. In Fig. 7 the ratio

$$R = \frac{2\bar{x}}{(x_{max}+x_{min})}, \tag{5}$$

obtained in this way is plotted against the successive short cycles n in the sense that the different points (open circles) represent its values over these cycles ("days"). We observe an overall oscillating pattern albeit with a high variability. Specifically, days where $x$ and $(x_{max}+x_{min})/2$ are very close and followed by days where deviations are substantial.

One may also compute $x$ from the analytic expression in Eq. (3). Since the average of the first term (in $\omega_1$) is identically zero we are left with

$$\begin{aligned}\bar{x}_n &= \frac{\varepsilon_2}{\sqrt{\lambda^2+\omega_2^2}}\frac{\omega_1}{2\pi}\int_{2\pi n/\omega_1}^{2\pi(n+1)/\omega_1} dt\,\sin(\omega_2 t-\phi_2+\psi_2)\\ &= \frac{\varepsilon_2}{\sqrt{\lambda^2+\omega_2^2}}\frac{\omega_1}{2\pi\omega_2}\left[\cos\left(\frac{2\pi n\omega_2}{\omega_1}-\phi_2+\psi_2\right)-\cos\left(\frac{2\pi(n+1)\omega_2}{\omega_1}-\phi_2+\psi_2\right)\right].\end{aligned} \tag{6}$$

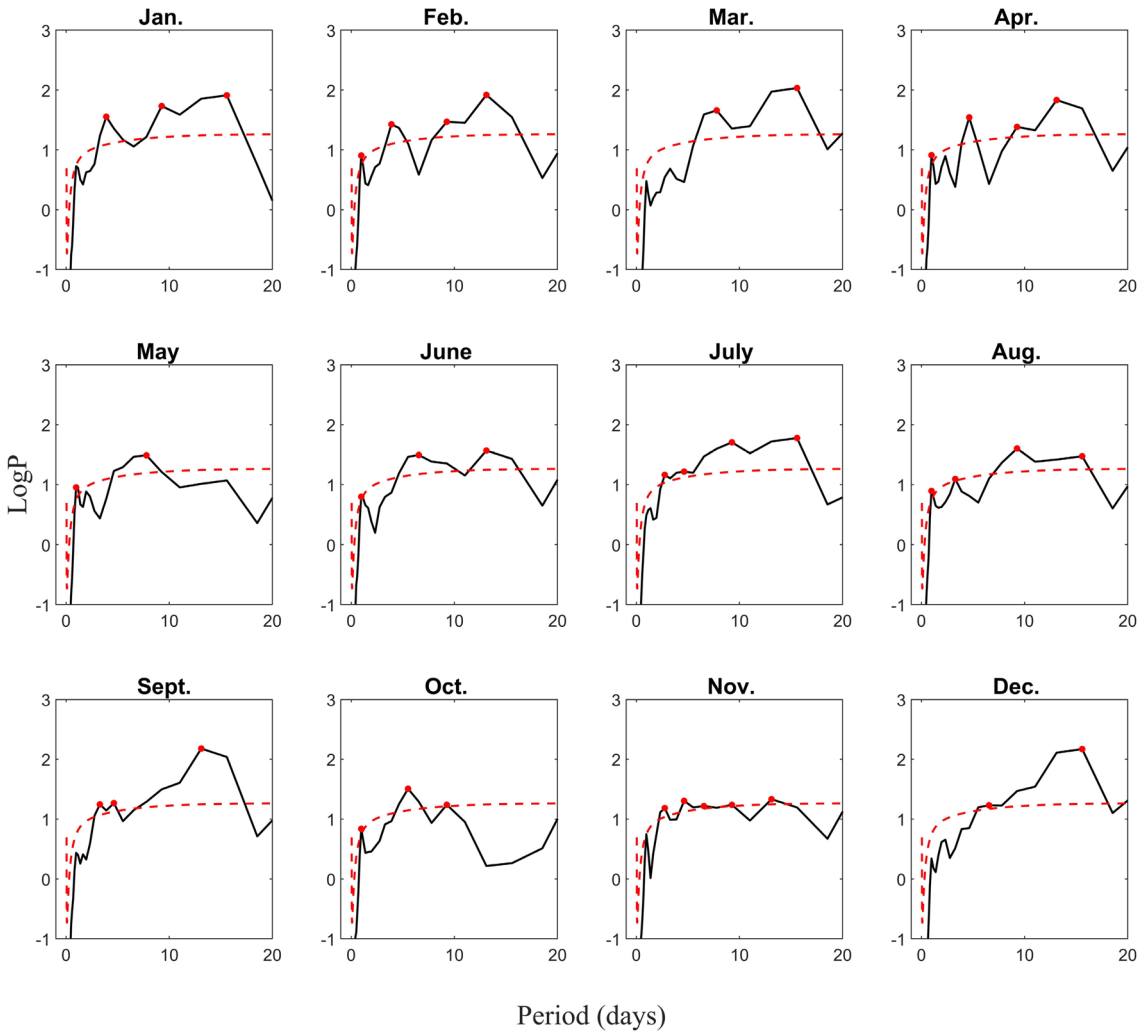


**Fig. 4** Same as Fig. 1 (third panel) but for all months in 2012

On the other hand, the analytical expression of the extremes during the successive short periods $T_1$ turns out to be intractable. We therefore limit ourselves to the numerical estimation of these quantities. Evaluating $x_n$ from (6) leads to results indistinguishable from those obtained numerically for the successive mean values of Fig. 7. In addition, expression (6) allows one to evaluate the effect of the phases $\varphi_1$, $\varphi_2$ as seen in Fig. 8.

Although the overall pattern is similar to Fig. 7 we observe differences in the form of a more wide distribution of $R$ over the cycles.

Coming back to Eqs. (3) and (5) one sees that deviations of $x_n$ from $(x_{max} + x_{min})/2$ tend to be masked if $\lambda$ is large and $\varepsilon_2$ small. The role of $\omega_2$ is subtler. In Fig. 9 we plot the ratio $R$ for a value of $\omega_2$ related irrationally to $\omega_1$. In this case the time series of $x(t)$ is quasi-periodic, bringing us closer to what one expects to find in the presence of natural variability. This is reflected in the ratio $R$, for which we observe in Fig. 9 a higher variability of values as compared to Figs. 7 and 8.

In summary, the presence of two forcings of different periods induces, generically, deviations of average temperature anomaly $x$ with respect to the value $(x_{max} + x_{min})/2$ taken over the short cycle. Interestingly, these deviations can overestimate or underestimate the mean value depending crucially on such factors as the frequencies and phases of the forcings. This result carries through straightforwardly to the case of three or more forcings. As mentioned in the introduction a recent empirical study (Bernhardt et al. 2018), using 215 first-order weather stations across the conterminous United States over the 30-year period 1981–2010, has shown statistically significant differences

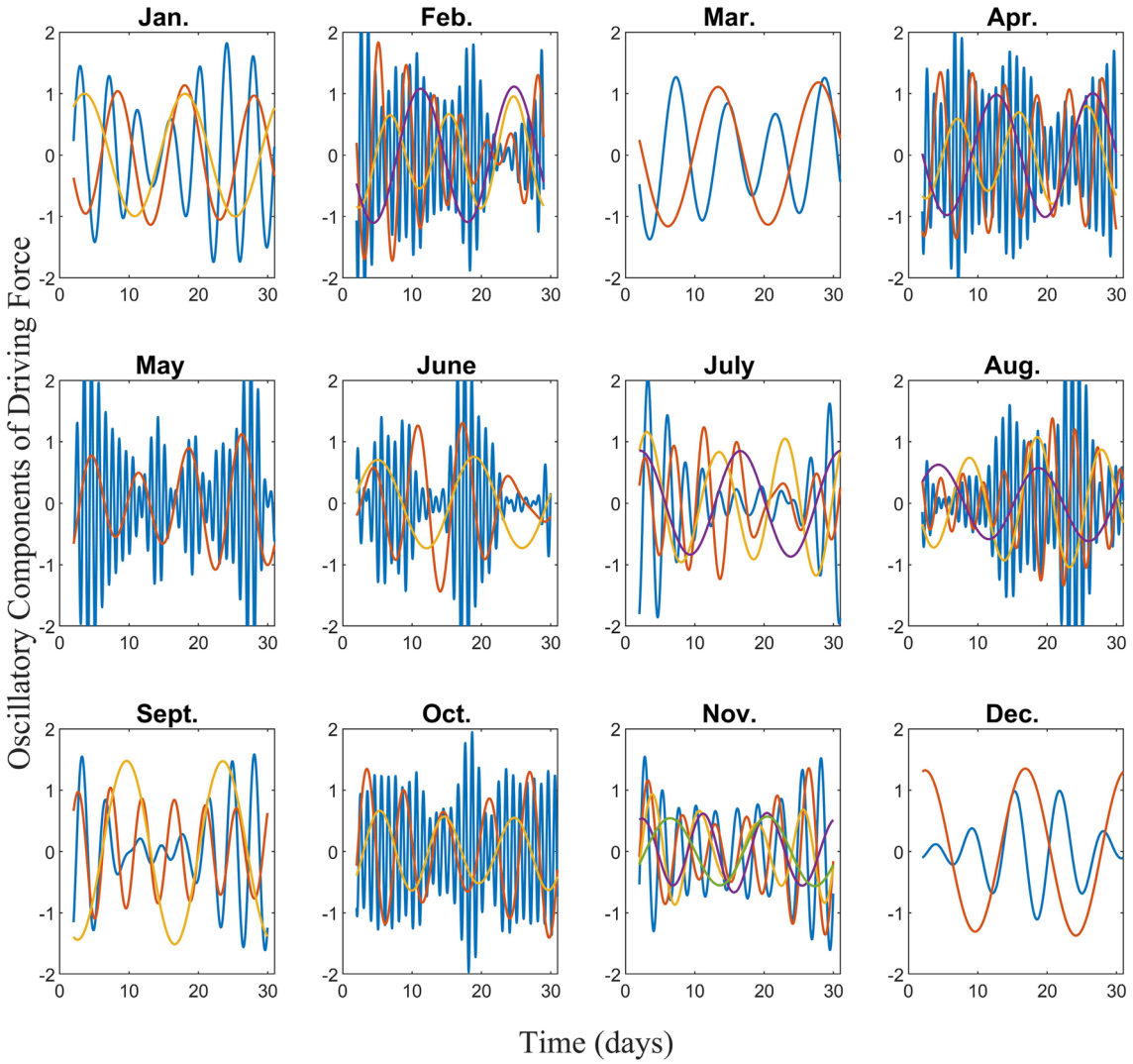


**Fig. 5** Same as Fig. 1 (bottom panel) but for all months in 2012

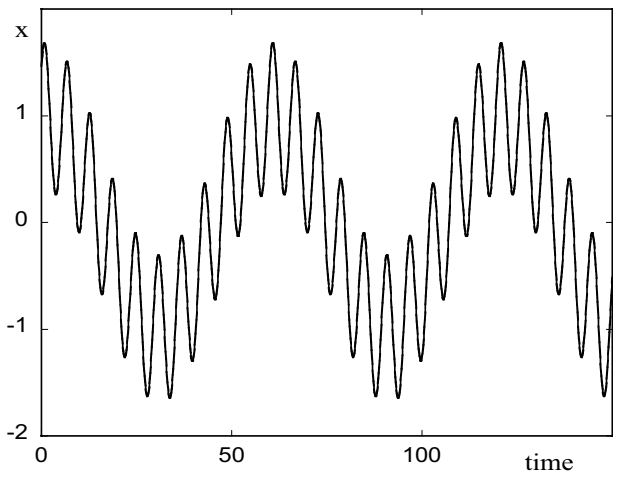


**Fig. 6** Time evolution of $x(t)$ as obtained numerically from Eq. (1) with $\lambda = \varepsilon_1 = \varepsilon_2 = 1$, $\omega_1 = \pi/3$ ($T_1 = 6$ time units), $\omega_2 = \omega_1/10$ ($T_2 = 60$ time units) and $\varphi_1 = \varphi_2 = 0$

between the two methods, with overestimation or underestimation of temperature by the traditional min–max method depending on the region and the time of the year. A demonstration of this result from the data analyzed in Sect. 2 here is presented in Figs. 10 and 11, which show a comparison between the two methods in the months of May and September. Overestimation and underestimation biases are visible.

Before concluding, we would like to point out that, regardless of the method to estimate the average daily temperature, there are cases where it is more appropriate to examine $T_{max}$ and $T_{min}$ separately, as they can reveal different signals in those two daily values, for example in the case of extreme events such as heat waves (Gershunov et al. 2009; Guirguis et al. 2017).

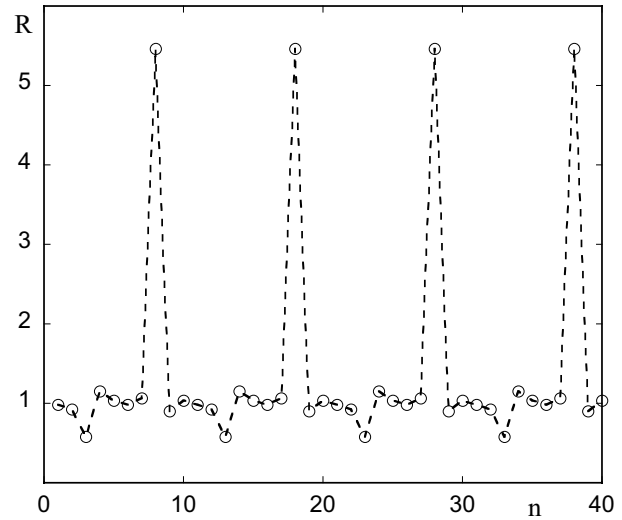


**Fig. 7** The ratio $R$ [Eq. (5)] as a function of the successive averaging periods n over the short cycle $\omega_1$. Parameter values as in Fig. 6

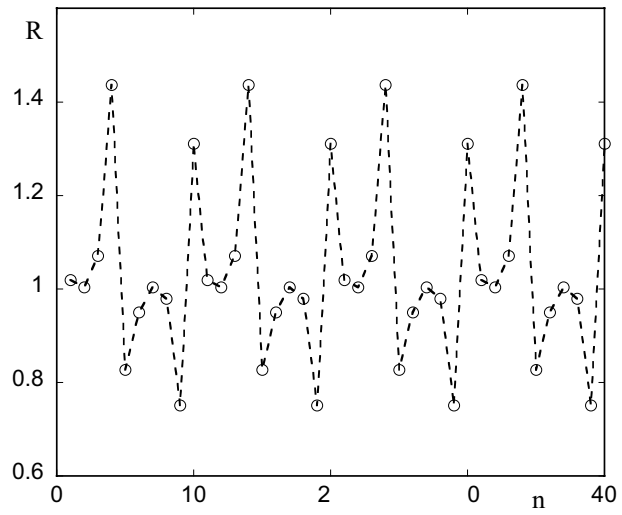


**Fig. 8** As in Fig. 7 but $\varphi 1 = \pi/2$ and $\varphi_2 = \pi/4$

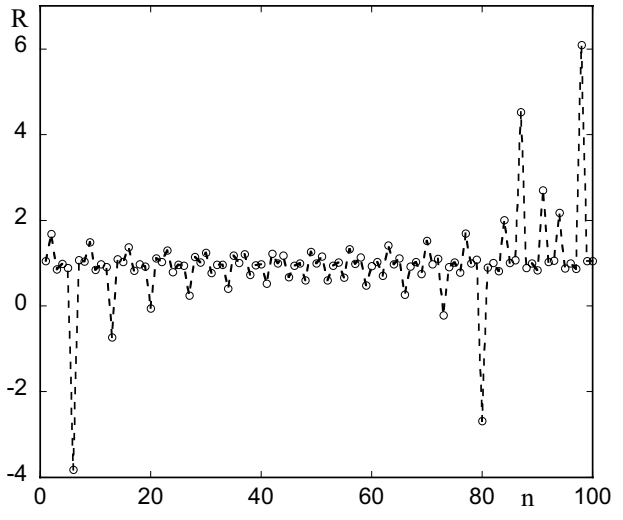


**Fig. 9** As in Fig. 8 but in the presence of two irrationally related frequencies $\omega_1 = \pi/3$ and $\omega_2 = \sqrt{2}\omega_1/16$

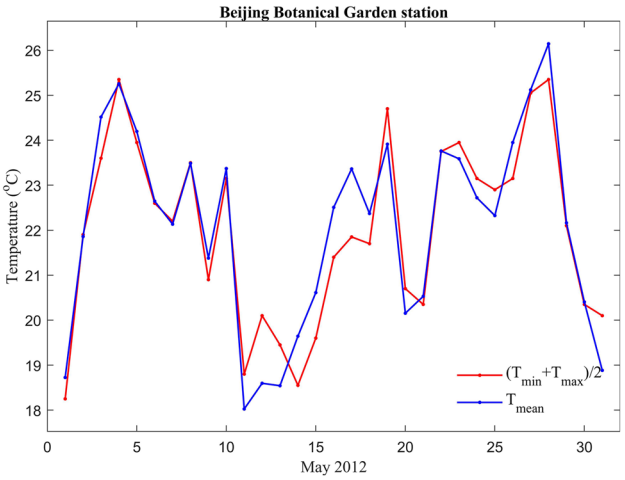


**Fig. 10** Comparison of the daily average temperature for the month of May 2012 at the Beijing Botanical Garden station using the two methods

## 4 Conclusions

Our analysis provides a dynamic explanation why there is no justification for using the (min + max)/2 method to estimate daily mean temperature, especially when hourly data are available. As we stated in the introduction this would be accurate only if the hourly temperature can be assumed a simple sinusoidal. Our data analysis reveals that in the hourly temperature data there exist slow driving forces superimposed on the daily cycle. These forces correspond to time scales/oscillations which make the hourly data clearly non-sinusoidal. As such, the (min + max)/2 method to estimate the mean daily temperature is inherently flawed. Theoretical arguments and a very recent study show that indeed

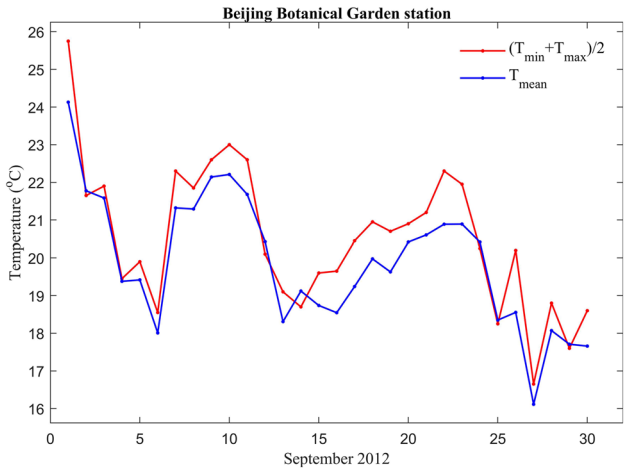


**Fig. 11** Same as Fig. 10 but for September 2012

the min–max methods may overestimate or underestimate the mean values based on regional climate variability.

**Acknowledgements** Part of this work was supported by the National Key R&D Program of China (2017YFC1501804), the National Natural Science Foundation of China (91737102 and 41575058).

## References

Berkes P, Wiskott L (2005) Slow feature analysis yields a rich repertoire of complex cells. J Vis 5(6):579–602

Bernhardt J, Carleton AM, LaMagna C (2018) A comparison of daily temperature-averaging methods: spatial variability and recent change for the CONUS. J Clim. https://doi.org/10.1175/jcli-d-17-0089.1

Dall'Amico M, Horsteiner M (2006) A simple method for estimating daily and monthly mean temperatures from daily minima and maxima. Int J Climatol 26:1929–1936

Gershunov A, Cayan DR, Iacobellis S (2009) The great heat wave over California and Nevada: signals of an increasing trend. J Clim 22:6181–6203

Guirguis K, Gershunov A, Cayan DR, Pierce D (2017) Heat wave probability in the changing climate of the Southwest US. Clim Dyn. https://doi.org/10.1007/s00382-017-3850-3

Ma Y, Guttorp P (2013) Estimating daily mean temperature from synoptic climate observations. Int J Climatol 33:1264–1269

Torrence C, Combo GP (1998) A practical guide to wavelet analysis. Bull Am Meteor Soc 79(1):61–78

Wiskott L (2003) Estimating driving forces of nonstationary time series with slow feature analysis. http://arxiv.org/abs/cond-mat/0312317/

Wiskott L, Sejnowski TJ (2002) Slow feature analysis: unsupervised learning of invariance. Neural Comput 14:715–770

Wiskott L et al (2011) Slow feature analysis. Scholarpedia 6(4):5282. https://doi.org/10.4249/scholapedia.5282

Yang P, Wang G, Zhang F, Zhou X (2015) Causality of global warming seen from observations: a scale analysis of driving force of the surface air temperature time series in the Northern Hemisphere. Clim Dyn. https://doi.org/10.1007/s00382-015-2761-4